

756 SUPPLEMENTARY MATERIAL: ADAPTING SELF-SUPERVISED  
 757 REPRESENTATIONS AS A LATENT SPACE FOR EFFICIENT GENERATION  
 758

759 A IMPLEMENTATION DETAILS  
 760

761 **Generative Decoder** Our generative decoder is implemented as a DiT-XL/2 (Peebles & Xie, 2023)  
 762 and trained for one million steps with a learning rate of  $10^{-4}$  using the AdamW (Loshchilov & Hutter,  
 763 2019) optimizer, a linear warm-up of 2000 steps and a global batch size of 512 on 8 H100 GPUs. Our  
 764 implementation uses RoPE (Su et al., 2023; Crowson et al., 2024), RMSNorm (Zhang & Sennrich  
 765 2019) and SwiGLU (Shazeer, 2020) activation functions, as we find that these modifications improve  
 766 the stability and performance of our generative decoder. We concatenate the SSL embedding to the  
 767 decoder patch tokens and apply full self-attention over all tokens.  
 768

769 **MLP Mixer** We adopt a standard MLP-Mixer (Tolstikhin et al., 2021) architecture, where all  
 770 conditioning information: CLIP text embeddings for text-to-image (T2I) generation and class tokens  
 771 for class-conditional image generation is concatenated with the noisy image token and passed through  
 772 the model. Our implementation follows the configuration provided by the *lucidrains* <sup>1</sup> GitHub  
 773 repository, with a hidden dimension of 1280, a depth of 28 layers, an expansion factor of 4 for the  
 774 channel MLP, and 2 for the token MLP.  
 775

776 B ADDITIONAL RESULTS  
 777

778 **Qualitative examples per token type.** As discussed in  
 779 the main paper, DINOv2 (Oquab et al., 2024) offers two  
 780 different types of tokens (besides patch tokens). First, the  
 781 standard `[cls]` token and additionally a set of register  
 782 tokens (Darcet et al., 2024). In Figure S3 we provide a  
 783 qualitative comparison of the differences in outcome be-  
 784 tween these two token types. We keep the SSL backbone  
 785 frozen and only train our generative decoder. We can ob-  
 786 serve that the `[reg]` token contains more knowledge about  
 787 appearance, location, and object orientation compared to  
 788 the `[cls]` token. However, none of the approaches gives  
 789 proper pixel-wise reconstructions, again highlighting the  
 790 need to integrate further information from the SSL encoder.



791 Figure S3: `[cls]` vs `[reg]` qualita-  
 792 tive comparison.

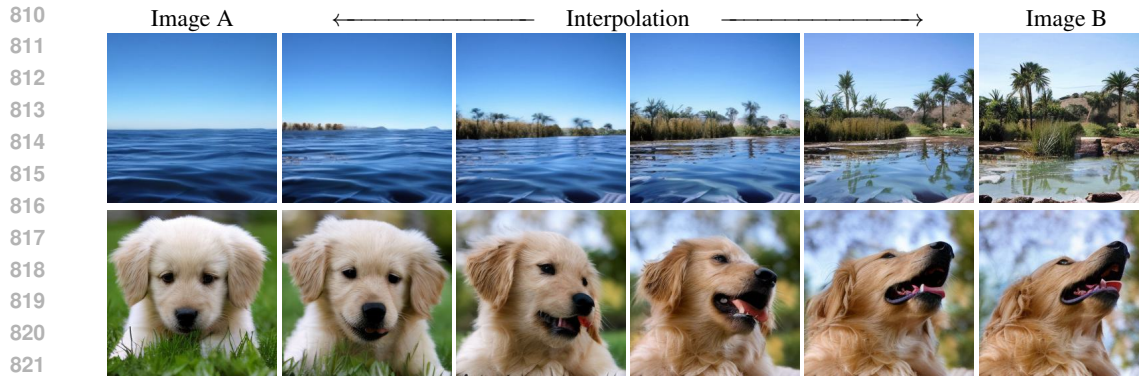
793 **Performance vs test-time compute.** Figure S2a shows  
 794 the number of function evaluations (NFE) vs reconstruction  
 795 FID (rFID) on the ImageNet (Deng et al., 2009) validation dataset. Performance improves with  
 796 increasing number of function evaluations (NFE), but saturates around 15–20. We hypothesize that  
 797 the strong conditioning signal from the generative decoder reduces the need for additional refinement  
 798 steps. Additionally, Figure S2b shows the generation performance depending on the number of  
 799 sampling steps. We see a continuous improvement with more NFE.

800 **Token type** DINOv2 (Oquab et al., 2024)  
 801 provides access to both a `[cls]` token and  
 802 a set of register tokens. We compare their  
 803 usefulness as latent representations for our  
 804 generative decoder in Table 5. Using a  
 805 frozen `[cls]` token results in strong re-  
 806 construction FID, indicating good semantic  
 807 alignment, but yields low pixel-level scores  
 808 such as PSNR and SSIM. In contrast, the  
 809 register token captures more fine-grained  
 visual details, improving pixel-wise reconstruction quality. This suggests that while the `[cls]` token emphasizes semantic content, the register token retains more low-level and regional information.

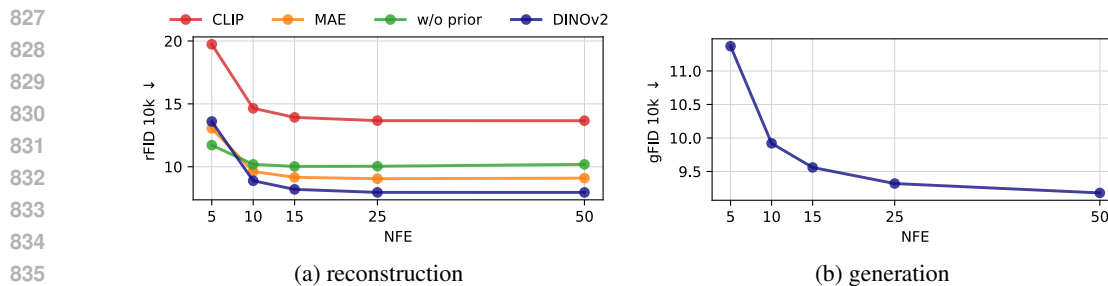
Table 5: **Ablation of token type.** Conditioning on DI-NOv2’s (Oquab et al., 2024) register tokens improves pixel-wise metrics, indicating stronger local information.

Token	rFID ↓	PSNR ↑	SSIM ↑	LPIPS ↓
<code>[reg]</code>	14.90	<b>12.85</b>	<b>29.07</b>	<b>0.52</b>
<code>[cls]</code>	<b>14.13</b>	12.59	28.41	0.54

<sup>1</sup><https://github.com/lucidrains/mlp-mixer-pytorch>



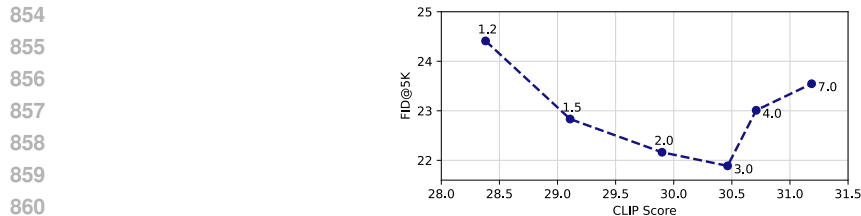
823 **Figure S1: More single token latent space interpolation results.** We observe smooth transitions  
824 not only in semantic content but also in object spatial configuration, and especially in object rotation  
825 (see dog).



838 **Figure S2: Effect of inference steps** for reconstruction and generation.

839 **More qualitative samples** We provide additional qualitative results to further illustrate the capabilities of our model: text-conditional generations are shown in Figure S9, and uncured class-conditional ImageNet generations in Figure S11.

844 **Additional Tokens** Some SSL encoders, such as DINOv2, provide additional global register tokens beyond the [cls] token. Incorporating these tokens increases latent capacity and improves reconstruction quality (see Figure S5 left). However, these tokens are typically unregularized and therefore do not inherit the favorable semantic and well-structured properties that our approach relies on. This also shows in the worse generative performance (gFID in Figure S5 right). Moreover, using multiple global tokens requires SSL models that have additional non-spatial tokens, as there is no straightforward way to repurpose spatial tokens into meaningful global representations. Given our focus on efficiency and structured single-token representations, we therefore restrict our method to the [cls] token, though multi-token extensions remain an interesting direction for future work.



861 **Figure S4: CFG effects on CLIP score and FID on the COCO (Lin et al., 2014) validation set.** As  
862 commonly observed, CLIP score increases with larger CFG scales, while FID improves only within a  
863 moderate range before rising again.

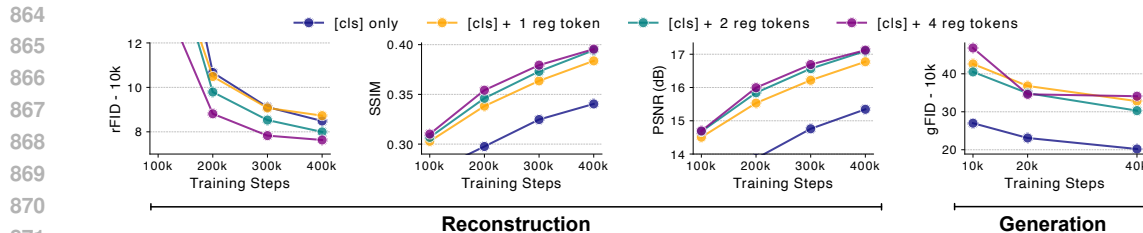


Figure S5: **Token number ablation.** Increasing the number of tokens in form of additional register tokens from DINOv2 [Darcet et al., (2024)] improves reconstruction quality. However, since register tokens do not have the favorable SSL properties, their space is not amenable for generation.

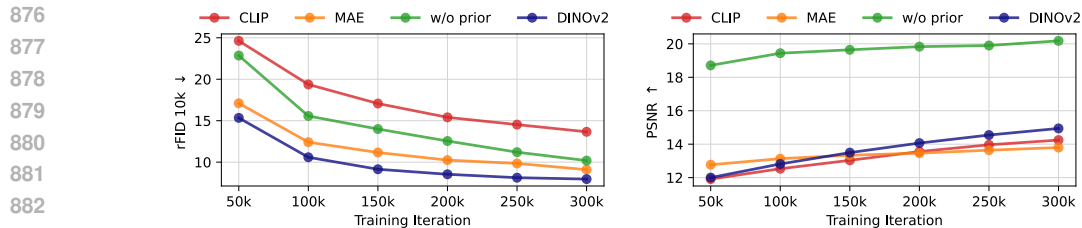


Figure S6: **Comparing SSL priors over training steps.** Our approach generalizes to different self-supervised methods. While the unregularized model without prior knowledge shows remarkable pixel-wise reconstruction, the latent space is not suitable for generation (see Table 4).

## C LIMITATIONS

While our single-token representation enables highly efficient generation and significant compute savings, it may limit expressiveness in capturing fine-grained details, particularly for complex or high-resolution scenes. Extending our approach to support richer multi-token representations while preserving efficiency is an interesting direction for future work. While our experiments demonstrate that the single-token embedding preserves certain low-level spatial structures, achieving fine-grained control over object location and scene composition remains an open challenge.

**Reconstruction-Generation trade-off** Another limitation of our method lies in the trade-off imposed by cosine similarity regularization. While stronger regularization enhances the smoothness and structure of the latent space, which is crucial for stable generative modeling, it can also suppress low-level detail, leading to degraded pixel-wise reconstructions. This trade-off may limit the applicability of our approach in scenarios where very high visual reconstruction fidelity is critical.

**Unleashing T2I for ImageNet-Pretrained Autoencoder** We investigate the capabilities of our Image-trained encoder-decoder framework. Figure S10 shows qualitative text-to-image samples. Despite being trained exclusively on ImageNet, the latent space does not overfit and shows strong generalization, generating diverse and high-quality images that extend well beyond the ImageNet manifold. Although the model generates plausible images, we find it struggles with compositional prompts that require placing multiple objects within a scene (e.g., a cat and a dog side-by-side). This limitation is expected, since the object-centric bias of ImageNet offers little exposure to multi-object scenes. However, finetuning our encoder on more diverse data alleviates this issue and enables the generation of multi-object content.

918  
 919  
 920  
 921  
 922  
 923  
 924  
 925  
 926  
 927  
 928  
 929  
 930  
 931  
 932  
 933  
 934  
 935  
 936  
 937  
 938  
 939  
 940  
 941  
 942  
 943  
 944  
 945  
 946  
 947  
 948  
 949  
 950  
 951  
 952  
 953  
 954  
 955  
 956  
 957  
 958  
 959  
 960  
 961  
 962  
 963  
 964  
 965  
 966  
 967  
 968  
 969  
 970  
 971

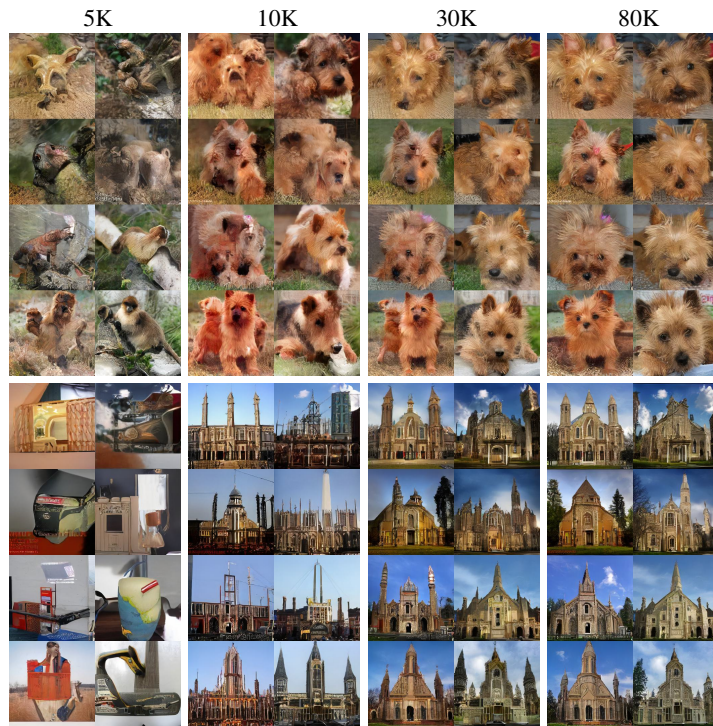


Figure S7: **Uncurated** class-conditional ImageNet generation results over training iterations (5k, 10k, 30k, and 80k). Note that our model produces good results as early as 30k training steps.

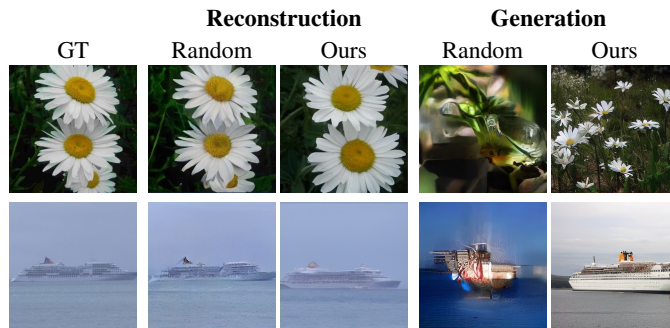


Figure S8: Qualitative comparison between a randomly-initialized encoder and ours. Generation refers to class-conditional samples with the same class as the corresponding GT image. While random initialization achieves stronger pixel-level reconstruction, it lacks the structured priors of pre-trained self-supervised encoders, resulting in poor generative performance. In contrast, our method balances reconstruction and generation.

972  
973  
974  
975  
976  
977  
978  
979  
980  
981  
982  
983  
984  
985  
986  
987  
988  
989  
990  
991  
992  
993  
994  
995  
996  
997  
998  
999  
1000  
1001  
1002  
1003  
1004  
1005  
1006  
1007  
1008  
1009  
1010  
1011  
1012  
1013  
1014  
1015  
1016  
1017  
1018  
1019  
1020  
1021  
1022  
1023  
1024  
1025

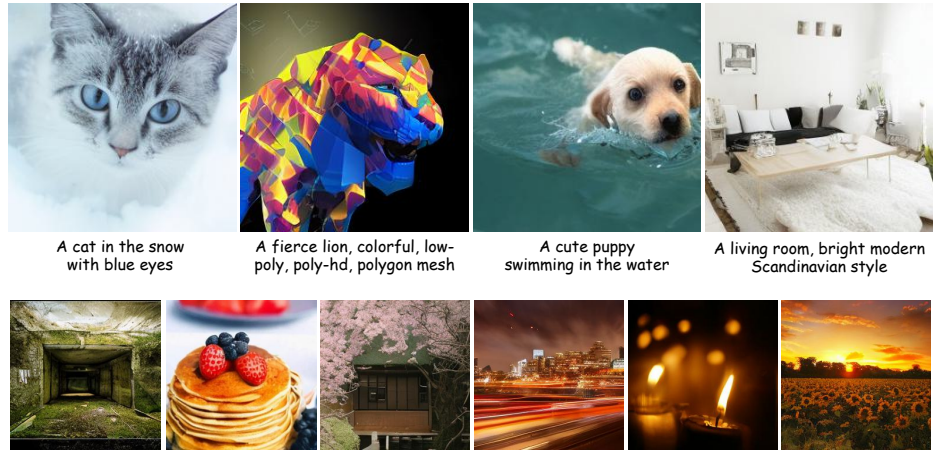


Figure S9: Additional text-to-image generation results with a CFG scale of 7.5 and RepTok encoder-decoder trained on the COYO dataset.



Figure S10: T2I generation results (CFG scale 3.5), using RepTok solely trained on ImageNet data with a latent space transformer. The autoencoder also transfers effectively to T2I tasks, producing visually compelling results.

1026  
1027  
1028  
1029  
1030  
1031  
1032  
1033  
1034  
1035  
1036  
1037  
1038  
1039  
1040  
1041  
1042  
1043  
1044  
1045  
1046  
1047  
1048  
1049  
1050  
1051  
1052  
1053  
1054  
1055  
1056  
1057  
1058  
1059  
1060  
1061  
1062  
1063  
1064  
1065  
1066  
1067  
1068  
1069  
1070  
1071  
1072  
1073  
1074  
1075  
1076  
1077  
1078  
1079



Figure S11: **Uncurated** class-conditional generation results of RepTok with CFG scale of 3.5.